의학석사 학위논문

Lamina Cribrosa Morphology in Glaucomatous Eyes with Hemifield Defect

시신경의 반측 결손을 보이는 녹내장안에서 사상판의 형태에 관한 고찰

2019 년 8 월

서울대학교 대학원
의학과 안과학 전공

김 지 아

Abstract

Lamina Cribrosa Morphology in Glaucomatous Eyes with Hemifield Defect

Ji-Ah Kim
Medicine, Department of ophthalmology
The Graduate School
Seoul National University

Purpose: To compare regional variations in lamina cribrosa (LC) curvature and depth between healthy eyes (Group 1) and naïve eyes with primary open-angle glaucoma (POAG) having superior (Group 2), inferior (Group 3), and both (Group 4) hemifield retinal nerve fiber layer (RNFL) defects.
Design: Cross-sectional study
Participants: Each group consisted of 39 eyes of 39 patients who were matched for age, sex, and axial length.
Methods: The LC curvature index (LCCI) and LC depth (LCD) were measured in B-scan images obtained using enhanced depth imaging optical coherence tomography at seven locations spaced equidistantly across the vertical optic disc diameter. Superior and inferior LCCI and LCD were compared by calculating the superior-to-inferior ratios (Sup/Inf ratio).
Main Outcome Measures: Comparisons of LCCI, LCD, and Sup/Inf ratio among the four groups.
Results: Compared with healthy eyes (group 1), LCCIs were larger at the superior and middle planes in group 2, at the inferior and middle planes in group 3, and at all planes in group 4 ($P \leq 0.004$). LCD showed similar results, but there was no difference in superior planes between groups 1 and 2. The Sup/Inf ratio of LCCI differed significantly between groups 1 (1.03) and 2 (1.20), groups 1 and 3 (0.79), groups 2 and 3, groups 2 and 4 (0.96),

and groups 3 and 4 (all $P < 0.001$), but not between groups 1 and 4 ($P = 0.273$). The Sup/Inf ratio of LCD differed only between groups 2 and 3 ($P = 0.002$).

Conclusions: Eyes with POAG showed regional differences in LC morphology, corresponding with the location of RNFL defects. The regional variations in LCCI suggest that LC morphology in POAG would be better assessed on a regional basis than by a global index.

Keyword : glaucoma, lamina cribrosa, hemifield detect

Student Number : 2017-21254

Table of Contents

Table

Figure

Chapter 1. Introduction

Glaucoma is characterized by the loss of retinal ganglion cells and their axons, resulting in corresponding visual field (VF) defects. According to the mechanical theory of glaucoma, posterior lamina cribrosa (LC) deformation is regarded as playing a central role in the development of glaucomatous optic neuropathy.[1] The posterior deformation and associated compression of the LC are thought to promote axonal and/or retinal ganglion cell damage through diverse mechanisms, including a blockade of axonal transport and tissue remodeling by reactive astrocytes.[2-5] Furthermore, compression of the LC may affect the diffusion of nutrients from the capillaries within the laminar beams to the adjacent axons, thereby further compromising the axons.[6]

Despite the importance of LC deformation, little is known about the relationship between glaucomatous axonal damage and LC deformation. For example, whether the LC deformation is a prerequisite for the development of glaucomatous axonal damage and what degree of LC deformation is required for the development of axonal damage are unclear. In addition, regional variations in LC deformation and their topographic relationship with axonal damage remain to be determined.

Eyes with early to moderate stage glaucoma often experience glaucomatous defects in only one hemifield. Because stress induced by increased intraocular pressure (IOP) is globally applied to the optic nerve head (ONH) within an eye, this phenomenon is intriguing. Previous studies have suggested a regional variability in connective tissue support of the axons (i.e., larger pores and thinner LC beams).[7-9] This variability may lead to differences in the vulnerability of areas of the LC to IOP-induced stress, resulting in a regional variability of LC deformation. That is, deformation may be greater in regions containing less dense connective tissue, resulting in greater damage to the corresponding region of optic disc.

From this perspective, determining the topographic relationship

between LC morphology and damage to the retinal nerve fiber layer (RNFL) may increase understanding of the importance of LC deformation in the development of glaucomatous axonal damage. In addition, such knowledge would provide a platform to develop a method to best assess LC morphology. This study therefore investigated the regional patterns of LC morphology in eyes with hemifield RNFL defects.

Chapter 2. Methods

This investigation was based on the Investigating Glaucoma Progression Study,[10, 11] an ongoing prospective investigation of glaucoma and healthy subjects at the Seoul National University Bundang Hospital Glaucoma Clinic. All subjects met the eligibility criteria of the Investigating Glaucoma Progression Study and provided written informed consent to participate. This study was approved by the Seoul National University Bundang Hospital Institutional Review Board and conformed to the Declaration of Helsinki.

2.1. Participants

Before the study, each patient underwent a complete ophthalmic examination, including assessments of visual acuity, refraction, slit-lamp biomicroscopy, gonioscopy, Goldmann applanation tonometry, and dilated stereoscopic examination of the optic disc, as well as measurements of corneal curvature (KR-1800; Topcon, Tokyo, Japan), central corneal thickness (CCT, Orbscan II; Bausch & Lomb Surgical, Rochester, NY, USA), and axial length (AXL, IOLMaster version 5; Carl Zeiss Meditec, Dublin, CA, USA). All subjects were also assessed by stereo disc photography, red-free fundus photography (Kowa VX-10; Kowa Medicals, Torrance, CA, USA), spectral domain optical coherence tomography (SD-OCT, Spectralis OCT; Heidelberg Engineering, Heidelberg, Germany), and

standard automated perimetry (Humphrey Field Analyzer II 750 and 24-2 Swedish interactive threshold algorithm; Carl Zeiss Meditec).

Subjects were included if they had a best-corrected visual acuity of at least 20/40, a spherical refraction of –8.0 to +3.0 diopters, and a cylinder correction within ±3.0 diopters. Primary open-angle glaucoma (POAG) was defined as the presence of glaucomatous optic nerve damage (i.e., neuroretinal rim thinning/notching and/or splinter hemorrhage and the presence of RNFL defect in the corresponding region) and associated VF defects without ocular diseases or conditions that may elevate IOP. RNFL defects identified by red-free photographs were confirmed by SD-OCT circumpapillary RNFL thickness. A glaucomatous VF change was defined as (1) a change outside the normal limit on the glaucoma hemifield test, (2) three abnormal points with a < 5% probability of being normal or one point with a < 1% probability of being normal by pattern deviation, or (3) a pattern standard deviation < 5% on two consecutive reliable tests. A VF measurement was considered reliable when both false-positive and false-negative rates were <25% and fixation losses were <20%.

Healthy subjects had an IOP ≤ 21 mm Hg with no history of increased IOP, an absence of glaucomatous disc appearance, no visible RNFL defect on red-free photography, and a normal VF. Absence of a glaucomatous disc appearance was defined as an intact neuroretinal rim without peripapillary hemorrhages, notches, or localized pallor. A normal VF was defined as the absence of glaucomatous VF defects and neurologic field defects.

Subjects with a history of previous intraocular surgery except uneventful cataract surgery or coexisting retinal (e.g., diabetic retinopathy, retinal vessel occlusion, or retinoschisis) or neurologic (e.g., pituitary tumor) diseases that could affect the VF were excluded from this study, as were patients with secondary (e.g., uveitic) glaucoma that could increase IOP. Eyes were also excluded when a good-quality image (i.e., quality score > 15) could not be obtained in more than five sections of enhanced depth

imaging (EDI) SD-OCT disc scans (when the quality score does not reach 15, the image-acquisition process automatically stopped, and the image of the respective sections is not obtained). Also excluded were eyes with a tilt ratio >1.3 between the longest and shortest diameters of the optic disc[12, 13] or torsion of the optic disc, defined as a torsion angle, calculated as the deviation of the long axis of the optic disc from the vertical meridian, >15º.[13, 14]

Subjects were divided into four groups. Group 1 consisted of healthy subjects, and groups 2–4 consisted of naïve POAG patients showing superior RNFL defects with corresponding inferior hemi VF defects (group 2), inferior RNFL defects with corresponding superior hemi VF defects (group 3), and both superior and inferior RNFL defects with corresponding inferior and superior VF defects (group 4). To be included in group 2 and 3, patients should have both RNFL defect and corresponding glaucomatous VF damage which were confined to single hemifield. There should be no RNFL defect or abnormal visual filed on the opposite hemifield in these groups. Subjects in the four groups were 1:1:1:1 by age, sex, and AXL.

2.2. Enhanced Depth Imaging OCT of the Optic Nerve Head

The optic nerve was imaged using the EDI technique of the Spectralis OCT system, a technique originally developed to visualize the full thickness of the choroid.[15] This technique yields images with a stronger signal and better image contrast in the deep ONH tissue than the conventional imaging technique.[16] Patients were imaged through undilated pupils using a rectangle subtending 10° × 15° of the optic disc. This rectangle was scanned with approximately 75 B-scan section images separated by 30–34 μm, with the scan line distance determined automatically by the machine. Approximately 42 SD-OCT frames were averaged for each section. This protocol provided the best trade-off between image quality and patient cooperation.[16] Potential magnification errors were avoided by entering the corneal curvature of each

eye into the Spectralis OCT system before scanning.

To enhance the visibility of the anterior LC surface, all disc scan images were post-processed using adaptive compensation,[17-19] and measurements performed using a manual caliper tool in Amira software (version 5.2.2, Visage Imaging, Berlin, Germany) by two experienced observers (J.A.K. and E.J.L.) who were masked to subjects' clinical information. The mean of measurements by the two observers were used for analysis. LC parameters on horizontal B-scan images were measured at 7 locations equidistant across the vertical optic disc diameter. Disc margin was defined as Bruch's membrane opening visible in the B-scan images. These seven B-scan lines were defined as planes 1 to 7 (top to bottom in Fig. 1), with planes 2 and 6 corresponding approximately to the mid-periphery, and planes 4 to the midhorizontal plane.

2.3. Measurement of Lamina Cribrosa Curvature Index

To quantify the posterior bowing of LC on the SD-OCT B-scan images, the LC curvature index (LCCI) was determined by assessing the inflection of a curve representing a section of the LC. LCCI was measured as described previously.[20, 21] In brief, the width (W) of Bruch's membrane (BM) opening (BMO) was measured in each B-scan, followed by measurement of the LC curve depth (LCCD) (Fig. 1). The BMO width was defined as the distance between the temporal and nasal termination points. Lines were drawn from each BM termination point perpendicular to the BMO reference line, until they met the anterior LC surface. The line connecting the two points on the anterior LC surface was the reference line for measuring the LCCD, which was defined as the maximum LC depth from the reference line (Fig. 1). The LCCI was calculated as (LCCD/W) × 100. Because the curvature was normalized to LC width, it describes the shape of the LC independent of the actual size of the ONH. Specifically, (LCCD/W) × 100 is a simple normalized measure that represents the posterior bowing or curvature of the

anterior LC surface within the BMO. Only the LC within the BMO was considered because the LC outside the BMO was often not clearly visible.

2.4. Measurement of Lamina Cribrosa Depth

To determine the LCD, a line connecting the edges of the BMO was set as a reference plane (BMO reference line), and the LCD was measured perpendicular to the reference plane at the maximally depressed point (Fig. 1).

2.5. Comparison of regional LC morphology

The superior and inferior LCCIs were compared by dividing the superior mean (average of plane 1 to 3) LCCI by the inferior mean (average of plane 5 to 7) LCCI (Sup/Inf ratio), with a ratio >1 indicating that the LC was more steeply curved in the superior than in the inferior ONH, and vice versa. LCCIs of planes 1 and 7, 2 and 6, and 3 and 5 were also compared by dividing superior LCCI by inferior LCCI (plane 1/7, 2/6, and 3/5 ratio, respectively). Superior and inferior LCD were compared similarly.

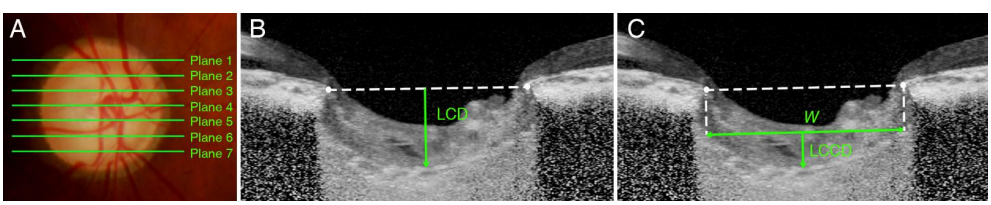

Fig. 1. Measurements of the lamina cribrosa (LC) depth (LCD) and LC curvature index (LCCI). (**A**) Disc photograph showing seven horizontal green lines indicating the locations at which the measurements were performed. (**B, C**) Enhanced depth imaging optical coherence tomography B-scan images obtained in plane 6 in (**A**). (**B**) The LCD was measured as the distance from the reference line connecting the two Bruch's membrane opening (BMO) points to the anterior surface of the LC. The LCD was measured at the maximally depressed point. (**C**) The LCCI was measured by dividing the LC curve depth (LCCD) by the width of the anterior LC surface reference line (*W*) and multiplying by 100.

2.6. Statistical Analysis

The inter-observer agreement for measuring LCCI and LCD was evaluated by calculating intraclass correlation coefficients (ICC). Differences in continuous variables among groups were compared by analysis of variance (ANOVA) with post hoc Tukey test, whereas categorical variables were compared using the Kruskal-Wallis test, with raw data subjected to Bonferroni correction based on the number of comparisons in each analysis. Linear regression analyses were performed to assess the associations between various clinical factors and LC parameters. Except where indicated otherwise, the data are presented as mean ± SD, and the cutoff for statistical significance was set at $P < 0.05$. All statistical analyses were performed using the Statistical Package for the Social Sciences software (version 22.0, SPSS, Chicago, IL, USA).

Chapter 3. Results

3.1. Demographic and Clinical Characteristics

This cross-sectional study initially involved 234 patients with POAG and 65 healthy subjects; of these, 54 and 13, respectively, were excluded due to the presence of a tilted disc. Twelve subjects were further excluded due to poor image quality, preventing the clear visualization of the anterior LC surface in at least two of the seven EDI-OCT B-scan disc images. After matching for age, sex, and AXL, each group consisted of 39 eyes of 39 subjects (total, 156 eyes).

Table 1 summarizes the demographic and clinical characteristics of the included subjects. IOP at the time of EDI-OCT was lower in Group 1 than the other 3 groups ($P = 0.002$). There were no significant differences in age, sex, spherical equivalent, CCT, AXL, blood pressure, migraine, and self-reported cold extremities.

Table 1. Demographic Characteristics of the Study Subjects

Variables	Group 1 (*n* = 39)	Group 2 (*n* = 39)	Group 3 (*n* = 39)	Group 4 (*n* = 39)	*P*-Value	Post hoc analysis
Age, y	55.9 ± 10.8	56.6 ± 10.9	56.1 ± 11.0	56.1 ± 10.8	0.994*	
Female, no. (%)	26 (66.7)	26 (66.7)	26 (66.7)	26 (66.7)	1.000†	
Spherical equivalent, D	-0.02 ± 1.45	-0.46 ± 1.66	-0.34 ± 1.52	-0.19 ± 1.66	0.641*	
Axial length, mm	23.9 ± 0.9	24.0 ± 1.0	23.8 ± 0.9	23.8 ± 0.9	0.822*	
Central corneal thickness, μm	554.7 ± 42.7	550.1 ± 36.6	548.1 ± 34.2	543.6 ± 33.3	0.608*	
Intraocular pressure, mmHg	12.4 ± 2.8	14.9 ± 4.8	14.8 ± 2.7	15.3 ± 3.9	**0.002***	1<2=3=4
Self-reported history of diabetes, no. (%)	4 (10.3)	4 (10.3)	3 (7.7)	2 (5.1)	0.821†	
Self-reported history of hypertension, no. (%)	6 (15.4)	14 (35.9)	16 (41.0)	13 (33.3)	0.082†	
Glaucoma family history, no. (%)	5 (15.4)	2 (5.1)	1 (2.6)	5 (15.4)	0.235†	
Migraine, no. (%)	8 (20.5)	8 (20.5)	7 (17.9)	2 (5.1)	0.213†	
Cold extremities, no. (%)	11 (28.2)	10 (25.6)	6 (15.4)	8 (20.5)	0.551†	
Systolic blood pressure, mmHg	125.3 ± 13.6	124.6 ± 14.0	128.3 ± 16.8	122.6 ± 10.3	0.333*	
Diastolic blood pressure, mmHg	71.8 ± 7.3	72.5 ± 9.5	75.5 ± 7.8	75.8 ± 7.6	0.064*	
Mean arterial pressure, mmHg	89.6 ± 8.4	89.9 ± 10.0	93.1 ± 9.7	91.4 ± 7.3	0.296*	
Mean ocular perfusion pressure, mmHg	51.5 ± 5.0	50.0 ± 7.3	52.3 ± 6.8	50.7 ± 5.4	0.400*	

Data are mean ± standard deviation values, with statistically significant *P*-values (< 0.05) in boldface. Statistical significance tested by *ANOVA and †Kruskal-Wallis test. Group 1 = healthy; Group 2 = naïve POAG with superior RNFL defect; Group 3 = naïve POAG with inferior RNFL defect; Group 4 = naïve POAG with both RNFL defects, D = diopters.

3.2. Differences in LCCI and LCD between glaucomatous and healthy eyes

Measurements of LCCI and LCD showed excellent intraobserver reproducibility, with ICC for LCCI of 0.979 (range, 0.970–0.986); and for LCD of 0.969 (range, 0.948–0.982).

Figure 2 shows the measured LCCI and LCD values in each group. Compared with healthy eyes (group 1), LCCI was larger in the superior and middle planes (planes 1–5) in group 2 (all $P \leq 0.003$), the inferior and middle planes (planes 4–7) in group 3 (all $P \leq 0.001$), and all planes in group 4 (all $P < 0.001$, Table 2).

LCD in all planes did not differ significantly in groups 1 and 2. Compared with group 1, LCD was significantly larger in the inferior planes (planes 5–7) in group 3 (all $P \leq 0.003$) and in all planes in group 4 (all $P \leq 0.005$, Table 2).

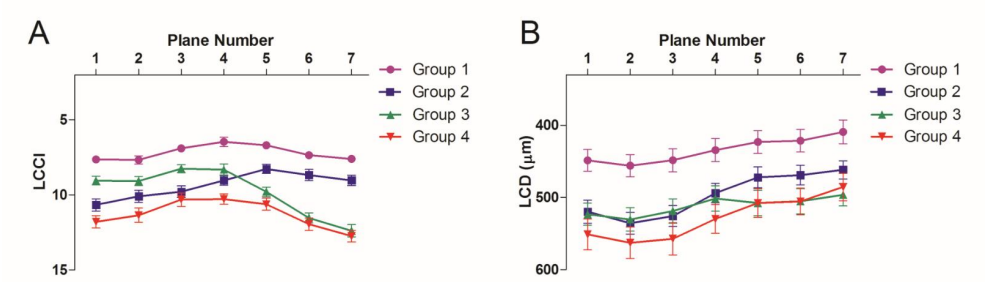

Fig. 2. Graph showing variations in lamina cribrosa (LC) curvature index (LCCI) and LC depth (LCD) in the different planes and groups. Error bars represent SEM. Group 1 = healthy; Group 2 = naïve POAG with superior RNFL defect; Group 3 = naïve POAG with inferior RNFL defect; Group 4 = naïve POAG with both RNFL defects.

Table 2. Comparison of Lamina Cribrosa Curvature Index (LCCI) and Lamina Cribrosa Depth (LCD) Between Healthy and POAG Eyes

LCCI								
Plane Number	Group 1: Healthy (n = 39)	Group 2: Superior Hemifield Defect (n = 39)	Group 3: Inferior Hemifield Defect (n = 39)	Group 4: Both Hemifield Defect (n = 39)	P-value	Post hoc analysis		
						Group 1 vs. Group 2	Group 1 vs. Group 3	Group 1 vs. Group 4
1	7.64 ± 1.26	10.68 ± 2.54	9.05 ± 1.83	11.80 ± 2.59	**<0.001**	**<0.001**	0.020	**<0.001**
2	7.68 ± 1.74	10.09 ± 2.57	9.08 ± 1.88	11.36 ± 2.93	**<0.001**	**<0.001**	0.043	**<0.001**
3	6.90 ± 1.47	9.79 ± 2.37	8.26 ± 1.65	10.32 ± 2.80	**<0.001**	**<0.001**	0.030	**<0.001**
4	6.47 ± 1.96	9.04 ± 2.03	8.32 ± 2.24	10.29 ± 2.21	**<0.001**	**<0.001**	**0.001**	**<0.001**
5	6.69 ± 1.35	8.28 ± 1.89	9.80 ± 1.98	10.63 ± 2.56	**<0.001**	**0.003**	**<0.001**	**<0.001**
6	7.35 ± 1.17	8.68 ± 2.29	11.54 ± 2.04	11.96 ± 2.61	**<0.001**	0.029	**<0.001**	**<0.001**
7	7.60 ± 1.29	9.03 ± 2.16	12.39 ± 2.55	12.76 ± 2.43	**<0.001**	0.021	**<0.001**	**<0.001**
LCD								
Plane Number	Group 1: Healthy (n = 39)	Group 2: Superior Hemifield Defect (n = 39)	Group 3: Inferior Hemifield Defect (n = 39)	Group 4: Both Hemifield Defect (n = 39)	P-value	Post hoc analysis		
						Group 1 vs. Group 2	Group 1 vs. Group 3	Group 1 vs. Group 4
1	448.69 ± 93.66	519.85 ± 99.59	523.31 ± 95.61	551.33 ± 133.41	**<0.001**	0.020	0.013	**<0.001**
2	456.08 ± 95.32	535.85 ± 93.65	530.56 ± 101.79	562.92 ± 135.71	**<0.001**	0.007	0.014	**<0.001**
3	448.54 ± 98.85	525.82 ± 90.54	518.92 ± 106.25	557.31 ± 139.29	**<0.001**	0.012	0.028	**<0.001**
4	434.41 ± 99.25	494.03 ± 83.06	501.54 ± 109.90	529.87 ± 124.30	**0.001**	0.064	0.028	**0.001**
5	423.33 ± 98.90	472.28 ± 89.68	507.92 ± 110.60	507.85 ± 123.05	**0.001**	0.180	**0.003**	**0.003**
6	421.54 ± 98.47	469.08 ± 84.89	505.36 ± 107.69	505.54 ± 115.45	**0.001**	0.174	**0.002**	**0.002**
7	409.26 ± 102.04	461.79 ± 78.34	496.31 ± 96.76	485.67 ± 117.35	**0.001**	0.096	**0.001**	**0.005**

Data are mean ± standard deviation values, with statistically significant P-values in boldface. Bonferroni correction was applied to raw data for measurements in the seven locations. Values that were significant after Bonferroni correction ($P < 0.007$; 0.05/7) are shown in bold. Statistical significance tested by ANOVA.

3.3. Regional Variations of LCCI

Mean Sup/Inf ratios in groups 1–4 were 1.03 ± 0.15, 1.20 ± 0.21, 0.79 ± 0.15, and 0.96 ± 0.19, respectively (Table 3, Figure 3). The Sup/Inf ratio was significantly higher in group 2 than in group 1 ($P < 0.001$) and was significantly lower in group 3 than in group 1 ($P < 0.001$). This ratio, however, did not differ significantly in groups 1 and 4.

Similar results were also observed for the plane 1/7 and plane 2/6 ratios, except that the latter did not differ significantly in groups 1 and 2. In contrast, plane 3/5 ratios differed significantly only between groups 1 and 3, groups 2 and 3, and groups 2 and 4 (all $P \leq 0.003$). Figure 4 shows representative eyes with superior and inferior RNFL defects.

3.4. Regional Comparisons of LCD

The Sup/Inf, plane 2/6, and plane 3/5 ratios differed significantly in groups 2 and 3 (all $P \leq 0.004$). The plane 3/5 ratio also differed significantly in groups 3 and 4, but there were no significant differences in other comparisons of regional LCD.

3.5. Factors associated with Sup/Inf ratios of LCCI and LCD

Linear regression analysis showed no covariates associated with the Sup/Inf and planes 1/7, 2/6, and 3/5 ratios (Table 4).

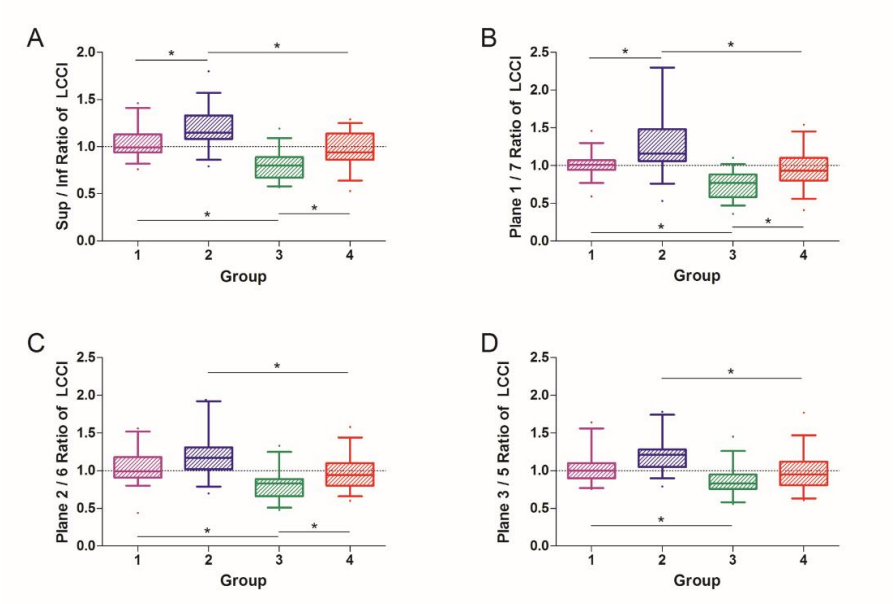

Fig. 3. Graph showing the (**A**) Sup/Inf, (**B**) plane 1/7, (**C**) plane 2/6, and (**D**) plane 3/5 ratios of the lamina cribrosa curvature index (LCCI). The box plots show the median, interquartile range, 95% percentile, and extreme values. There was no significant difference in Sup/Inf ratio between groups 1 and 4. Group 2 had a larger, and group 3 had a smaller, Sup/Inf ratio than groups 1 and 4. The between group differences in LCCI ratios corresponded with the location of RNFL defects. Group 1 = healthy; Group 2 = naïve POAG with superior RNFL defect; Group 3 = naïve POAG with inferior RNFL defect; Group 4 = naïve POAG with both RNFL defects. * Bonferroni-corrected $P < 0.013$, ANOVA.

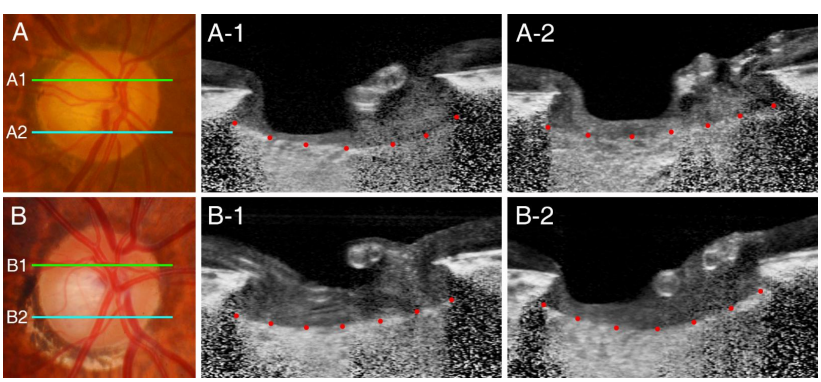

Fig. 4. Representative eyes with superior (**A**) and inferior (**B**) rim thinning from a 69- and a 72-year old man, respectively. (**A-1, B-1**) Superior B-scan images at plane 2, indicated by the *green* line in the optic disc photographs. (**A-2, B-2**) Inferior B-scan images at plane 6, indicated by the *blue* line in the optic disc photographs. Note that the LC curvature was noticeably steeper at the hemisphere with rim thinning in both eyes. The LCCIs in panels A1, A2, B1 and B2 were 11.75, 8.02, 8.39, and 13.32, respectively.

Table 3. Comparison of Superior / Inferior Ratio of Lamina Cribrosa Curvature Index (LCCI) and Lamina Cribrosa Depth (LCD) Between Healthy and POAG eyes

LCCI												
Plane Ratio	Group 1: Healthy (n = 39)	Group 2: Superior Hemifield Defect (n = 39)	Group 3: Inferior Hemifield Defect (n = 39)	Group 4: Both Hemifield Defect (n = 39)	P-value	Post hoc analysis					
						Group 1 vs. Group 2	Group 1 vs. Group 3	Group 1 vs. Group 4	Group 2 vs. Group 3	Group 2 vs. Group 4	Group 3 vs. Group 4
Superior Mean / Inferior Mean Ratio	1.03 ± 0.15	1.20 ± 0.21	0.79 ± 0.15	0.96 ± 0.19	**< 0.001**	**< 0.001**	**< 0.001**	0.273	**< 0.001**	**< 0.001**	**<0.001**
Plane 1 / 7 Ratio	1.02 ± 0.16	1.26 ± 0.37	0.75 ± 0.18	0.96 ± 0.26	**< 0.001**	**< 0.001**	**< 0.001**	0.687	**< 0.001**	**< 0.001**	**0.003**
Plane 2 / 6 Ratio	1.05 ± 0.23	1.20 ± 0.27	0.80 ± 0.19	0.97 ± 0.23	**< 0.001**	0.029	**< 0.001**	0.421	**< 0.001**	**< 0.001**	**0.008**
Plane 3 / 5 Ratio	1.06 ± 0.32	1.20 ± 0.22	0.86 ± 0.19	0.99 ± 0.26	**< 0.001**	0.085	**0.002**	0.623	**< 0.001**	**0.003**	0.084
LCD												
Plane Ratio	Group 1: Healthy (n = 39)	Group 2: Superior Hemifield Defect (n = 39)	Group 3: Inferior Hemifield Defect (n = 39)	Group 4: Both Hemifield Defect (n = 39)	P-value	Post hoc analysis					
						Group 1 vs. Group 2	Group 1 vs. Group 3	Group 1 vs. Group 4	Group 2 vs. Group 3	Group 2 vs. Group 4	Group 3 vs. Group 4
Superior Mean / Inferior Mean Ratio	1.09 ± 0.11	1.13 ± 0.09	1.05 ± 0.10	1.12 ± 0.10	**0.002**	0.232	0.317	0.625	**0.002**	0.898	0.021
Plane 1 / 7 Ratio	1.12 ± 0.17	1.13 ± 0.15	1.07 ± 0.14	1.14 ± 0.13	0.127						
Plane 2 / 6 Ratio	1.09 ± 0.12	1.15 ± 0.12	1.06 ± 0.12	1.11 ± 0.11	**0.008**	0.128	0.613	0.853	**0.004**	0.503	0.183
Plane 3 / 5 Ratio	1.06 ± 0.09	1.12 ± 0.12	1.03 ± 0.08	1.10 ± 0.10	**<0.001**	0.044	0.349	0.425	**<0.001**	0.675	**0.009**

Data are mean ± standard deviation values, with statistically significant P-values in boldface. Values that were significant after Bonferroni correction (P < 0.013; 0.05/4) are shown in bold. Statistical significance tested by ANOVA.

Table 4. Factors Associated with the Mean Superior / Inferior Lamina Cribrosa Curvature Index (LCCI) and Lamina Cribrosa Depth (LCD) ratio

	Superior / Inferior LCCI ratio				Superior / Inferior LCD ratio			
	Healthy		POAG		Healthy		POAG	
Variables	β	*P*	β	*P*	β	*P*	β	*P*
Age, *per 1 yr older*	0.001	0.565	0.001	0.760	0.001	0.975	0.001	0.186
Male gender	0.059	0.254	0.028	0.568	-0.003	0.945	0.008	0.676
SE, *per 1 D larger*	-0.004	0.828	-0.010	0.509	-0.011	0.387	0.008	0.172
AXL, *per 1 mm larger*	0.039	0.162	0.002	0.939	-0.006	0.753	-0.008	0.467
CCT, *per 1 μm larger*	0.000	0.822	0.001	0.071	0.001	0.902	0.000	0.223
Baseline IOP, *per 1 mmHg higher*	0.011	0.189	0.006	0.316	0.006	0.359	-0.002	0.499
Self-reported diabetes	0.032	0.695	0.034	0.690	-0.034	0.559	0.009	0.793
Self-reported hypertension	0.023	0.735	0.010	0.830	-0.054	0.262	0.019	0.332
Family history of glaucoma	-0.113	0.115	0.028	0.758	0.026	0.627	0.005	0.901
Migraine	-0.034	0.570	-0.043	0.508	-0.037	0.398	-0.038	0.161
Cold extremities	-0.072	0.178	0.018	0.746	0.030	0.440	-0.003	0.914
Systolic blood pressure, *per 1 mmHg higher*	-0.001	0.639	0.000	0.847	-0.002	0.229	-0.001	0.173
Diastolic blood pressure, *per 1 mmHg higher*	0.003	0.381	-0.003	0.267	-0.003	0.281	-0.002	0.065
Location of RNFL defect	N/A	N/A	-0.120	**< 0.001**	N/A	N/A	-0.008	0.499

POAG, primary open angle glaucoma; SE, spherical equivalent; D, diopters; AXL, axial length; CCT, central corneal thickness; IOP, intraocular pressure; RNFL, retinal nerve fiber layer.

Chapter 4. Discussion

The present study demonstrated regional differences in LC curvature in POAG eyes differing in their locations of RNFL/VF defects. LC curvature was greater at the planes corresponding to the location of the RNFL defect. To our knowledge, this study is the first to correlate the location of the RNFL defect and regional variations in LC morphology.

Because LC morphology is highly variable on vertical and radial scans, LCCI and LCD in the present study were measured using horizontal B-scan images. A horizontal ridge at or near the mid-horizontal ONH[22] results in the anterior LC surface having a W-shaped configuration in vertical and oblique scans (i.e., the LC would have at least two separate curvatures (Supplementary Video S1)). Therefore, analysis of the LC configuration using vertical or oblique scans would be complicated.[21] In contrast, the LC has a relatively regular configuration in the horizontal plane, with a flat or U shaped appearance with different regional steepness, allowing the measurement of LCCI (Supplementary Video S2).[21]

Regional differences in LC morphology were analyzed by measuring the Sup/Inf ratios of LC indexes as well as their absolute values, thereby compensating for innate interindividual variations in LCD and LCCI. Subjects with a higher initial LCCI or LCD would have higher subsequent LCCI or LCD despite a lower degree of posterior LC deformation. Thus, only comparing absolute values may lead to erroneous conclusions.

Plane 4 was considered as the midhorizontal plane in all patients. This idea was based on the assumption that the ONH is symmetric (i.e., the horizontal ridge is located at the geometric midhorizon). However, this may not be the case in all patients. Such variation may have affected the result. The more obvious difference of LCCI between plane 1 and 7 (planes most farther from the midhorizontal plane) than between plane 3 and 5 (planes closest to the midhorizontal plane) may be partly attributed to this matter.

The patient classification was based on the presence of RNFL defect and corresponding VF defect in one hemifield or both hemifields. In this process, patients who had an RNFL defect without corresponding VF damage (i.e., preperimteric RNFL defect) in any hemifield were not included in the analysis. However, it is possible that some patients included in group 2 or 3 might have started early glaucomatous change in the opposite hemifield that was not detected by red-free photography or OCT. In other words, the glaucomatous damage might have not been completely limited to one hemifield in some patients in group 2 and 3. This should be considered when interpreting the result of the current study.

Damage to the optic nerve in glaucoma occurs preferentially in the superior or inferior region. This tendency toward regional glaucomatous damage may result from regional variations in the LC (i.e., larger pores and thinner LC beams in the superior and inferior peripheral regions than in the central region).[7-9] Our findings are in line with this concept and provide insight into the relationship between LC density and axonal damage.

The present study demonstrated that the LCCI was greater at the location of axonal damage. Although regional LCCI variation may be innate, larger LCCI can be derived from acquired bowing induced by translaminar pressure difference (TLPD). This idea is supported by the finding that LCCI is larger in eyes with higher IOP[20] and varies depending on the level of IOP within an individual.[23] LCCI can indicate the position of the LC due to native IOP at the moment of the scan, or can change over time with age or due to glaucomatous connective tissue remodeling or both. Assuming that large LCCI reflects greater LC bowing, our finding may suggest that the regional variability of LC exists in terms of susceptibility to TLPD. The degree of regional LC deformation is probably affected by the material property of the LC at that region.[24] That is, posterior LC deformation would occur first in the region of lower density. Taken together, these findings suggest the possibility that posterior LC deformation first occurs at the

location of least dense LC, leading to subsequent development of glaucomatous axonal damage at the corresponding location.

LC evaluation may have clinical value. Studies have shown that assessment of LC morphology may be useful in the differential diagnosis of glaucoma from other optic neuropathies[25] and predict disease outcome.[26, 27] The current study demonstrated that LC curvature varied depending on horizontal planes within single ONH, being prominent in the region corresponding to RNFL damage. This finding suggests that it may be better to evaluate LC curvature on a regional rather than a global basis, as global evaluation may miss small degrees of localized LC deformation.

LCD also showed intergroup differences. However, there were no significant differences between groups 1 and 2 at the superior location. LCD is larger in the superior than in the inferior planes in both healthy and glaucomatous eyes.[28-30] Therefore, the same degree of LC deepening would result in smaller proportional changes in the superior than in the inferior region and may explain the lack of significant difference in the superior planes.

The LCCI ratios comparing superior and inferior regions showed differences between all pairs of groups except groups 1 and 4. However, LCD ratios differed only for groups 2 and 3, likely because of the opposite locations of their RNFL defects. This finding is likely associated with the limited ability of LCD to characterized glaucomatous LC morphology as demonstrated previously.[20, 21] Because the LCD was measured from the BMO, it should be influenced by the choroidal thickness, which varies among individuals.[31] The LC is a sieve-like perforation in the posterior part of the sclera and is sustained by load-bearing connective tissues of the peripapillary sclera. Thus, including the choroidal thickness in the LCD would lead to a biased assessment of LC morphology.[20, 32]

This study had several limitations. First, a LC surface reference line from the LC insertion points may have allowed a more precise

quantification of the LC curve. However, in measuring the LC curve, the present study included only the LC within the BMO width, because the LC was often not visible outside this region. However, we previously demonstrated that the LCCI measured using the entire LC (i.e. between the LC insertions) was comparable to that measured on the LC within the BMO in eyes with an LC visible up to the LC insertion.[23] Thus, the LC curve within the BMO is representative of the actual LC curve. Second, we referred to the bowed LC configuration as LC curvature; however, the curvature is a geometric entity that refers to the inverse of the radius of the arc of a circle best fitting the portion of the curve. Thus, LCCI should not be considered a parameter corresponding to an actual LC curvature, suggesting the need for further study to investigate the method of calculating the actual curvature of the LC.[23] Third, because eyes with a tilted or torted optic disc were excluded, our findings cannot be directly applied to eyes with these conditions. Fourth, LCCI was measured only in horizontal scans. As described above, this was to avoid the complexity in the analysis of LCCI using the vertical scan. However, LCCI in vertical scan may provide additional information that may help assess the LC curvature more comprehensively. Finally, this study included only Korean patients, and so it is possible that the present findings cannot be extrapolated to other ethnic populations.

In conclusion, regional differences in LC morphology, which corresponded with the location of the RNFL defect, were observed in eyes with POAG. This finding is in accord to the concept that deformation of the LC is a principal event in the development of glaucomatous optic neuropathy. The regional variations of the LCCI suggested the need to assess LC morphology on a regional rather than a global basis in eyes with POAG.

Bibliography

1. Quigley HA, Addicks EM, Green WR, Maumenee AE. Optic nerve damage in human glaucoma. Ii. The site of injury and susceptibility to damage. *Arch Ophthalmol* 1981;99(4):635-649.
2. Anderson DR, Hendrickson A. Effect of intraocular pressure on rapid axoplasmic transport in monkey optic nerve. *Invest Ophthalmol* 1974;13(10):771-783.
3. Minckler DS, Bunt AH, Johanson GW. Orthograde and retrograde axoplasmic transport during acute ocular hypertension in the monkey. *Invest Ophthalmol Vis Sci* 1977;16(5):426-441.
4. Minckler DS, Tso MO. A light microscopic, autoradiographic study of axoplasmic transport in the normal rhesus optic nerve head. *Am J Ophthalmol* 1976;82(1):1-15.
5. Hernandez MR. The optic nerve head in glaucoma: Role of astrocytes in tissue remodeling. *Prog Retin Eye Res* 2000;19(3):297-321.
6. Burgoyne CF, Downs JC, Bellezza AJ, Suh JK, Hart RT. The optic nerve head as a biomechanical structure: A new paradigm for understanding the role of iop-related stress and strain in the pathophysiology of glaucomatous optic nerve head damage. *Prog Retin Eye Res* 2005;24(1):39-73.
7. Quigley HA, Addicks EM. Regional differences in the structure of the lamina cribrosa and their relation to glaucomatous optic nerve damage. *Arch Ophthalmol* 1981;99(1):137-143.
8. Quigley HA, Hohman RM, Addicks EM, Massof RW, Green WR. Morphologic changes in the lamina cribrosa correlated with neural loss in open-angle glaucoma. *Am J Ophthalmol* 1983;95(5):673-691.
9. Jonas JB, Mardin CY, Schlotzer-Schrehardt U, Naumann GO. Morphometry of the human lamina cribrosa surface. *Invest Ophthalmol Vis Sci* 1991;32(2):401-405.

10. Kim YW, Lee EJ, Kim TW, Kim M, Kim H. Microstructure of beta-zone parapapillary atrophy and rate of retinal nerve fiber layer thinning in primary open-angle glaucoma. *Ophthalmology* 2014;121(7):1341-1349.
11. Choi YJ, Lee EJ, Kim BH, Kim TW. Microstructure of the optic disc pit in open-angle glaucoma. *Ophthalmology* 2014;121(11):2098-2106 e2092.
12. Jonas JB, Papastathopoulos KI. Optic disc shape in glaucoma. *Graefes Arch Clin Exp Ophthalmol* 1996;234 Suppl 1:S167-173.
13. Vongphanit J, Mitchell P, Wang JJ. Population prevalence of tilted optic disks and the relationship of this sign to refractive error. *Am J Ophthalmol* 2002;133(5):679-685.
14. Samarawickrama C, Mitchell P, Tong L, et al. Myopia-related optic disc and retinal changes in adolescent children from singapore. *Ophthalmology* 2011;118(10):2050-2057.
15. Spaide RF, Koizumi H, Pozzoni MC. Enhanced depth imaging spectral-domain optical coherence tomography. *Am J Ophthalmol* 2008;146(4):496-500.
16. Lee EJ, Kim TW, Weinreb RN, et al. Visualization of the lamina cribrosa using enhanced depth imaging spectral-domain optical coherence tomography. *Am J Ophthalmol* 2011;152(1):87-95 e81.
17. Girard MJ, Tun TA, Husain R, et al. Lamina cribrosa visibility using optical coherence tomography: Comparison of devices and effects of image enhancement techniques. *Invest Ophthalmol Vis Sci* 2015;56(2):865-874.
18. Girard MJ, Strouthidis NG, Ethier CR, Mari JM. Shadow removal and contrast enhancement in optical coherence tomography images of the human optic nerve head. *Invest Ophthalmol Vis Sci* 2011;52(10):7738-7748.
19. Mari JM, Strouthidis NG, Park SC, Girard MJ. Enhancement of lamina cribrosa visibility in optical coherence tomography images using adaptive compensation. *Invest Ophthalmol Vis Sci* 2013;54(3):2238-2247.

20. Lee SH, Kim TW, Lee EJ, Girard MJ, Mari JM. Diagnostic power of lamina cribrosa depth and curvature in glaucoma. *Invest Ophthalmol Vis Sci* 2017;58(2):755-762.
21. Lee EJ, Kim T-W, Kim H, et al. Comparison between lamina cribrosa depth and curvature as a predictor of progressive retinal nerve fiber layer thinning in primary open-angle glaucoma. *ophthalmology glaucoma* 2018;In press.
22. Park SC, Kiumehr S, Teng CC, et al. Horizontal central ridge of the lamina cribrosa and regional differences in laminar insertion in healthy subjects. *Invest Ophthalmol Vis Sci* 2012;53(3):1610-1616.
23. Lee SH, Yu DA, Kim TW, et al. Reduction of the lamina cribrosa curvature after trabeculectomy in glaucoma. *Invest Ophthalmol Vis Sci* 2016;57(11):5006-5014.
24. Quigley HA, Dorman-Pease ME, Brown AE. Quantitative study of collagen and elastin of the optic nerve head and sclera in human and experimental monkey glaucoma. *Curr Eye Res* 1991;10(9):877-888.
25. Lee EJ, Choi YJ, Kim TW, Hwang JM. Comparison of the deep optic nerve head structure between normal-tension glaucoma and nonarteritic anterior ischemic optic neuropathy. *PLoS One* 2016;11(4):e0150242.
26. Lee EJ, Kim TW, Kim M, Kim H. Influence of lamina cribrosa thickness and depth on the rate of progressive retinal nerve fiber layer thinning. *Ophthalmology* 2015;122(4):721-729.
27. Lee EJ, Kim TW. Lamina cribrosa reversal after trabeculectomy and the rate of progressive retinal nerve fiber layer thinning. *Ophthalmology* 2015;122(11):2234-2242.
28. Park SC, Brumm J, Furlanetto RL, et al. Lamina cribrosa depth in different stages of glaucoma. *Invest Ophthalmol Vis Sci* 2015;56(3):2059-2064.

29. Seo JH, Kim TW, Weinreb RN. Lamina cribrosa depth in healthy eyes. *Invest Ophthalmol Vis Sci* 2014;55(3):1241-1251.

30. Kim JA, Kim TW, Weinreb RN, et al. Lamina cribrosa morphology predicts progressive retinal nerve fiber layer loss in eyes with suspected glaucoma. *Sci Rep* 2018;8(1):738.

31. Rhodes LA, Huisingh C, Johnstone J, et al. Peripapillary choroidal thickness variation with age and race in normal eyes. *Invest Ophthalmol Vis Sci* 2015;56(3):1872-1879.

32. Vianna JR, Lanoe VR, Quach J, et al. Serial changes in lamina cribrosa depth and neuroretinal parameters in glaucoma: Impact of choroidal thickness. *Ophthalmology* 2017;124(9):1392-1402.

국문초록

시신경의 반측 결손을 보이는 녹내장안에서 사상판의 형태에 관한 고찰

김지아
서울대학교 대학원
의학과 안과학전공

목 적: 정상군 (그룹 1), 치료받지 않은 일차개방각녹내장 중 상측 (그룹 2), 하측 (그룹 3), 그리고 양측 (그룹 4)의 시신경 결손을 보이는 환자들에서 사상판의 깊이와 휘어진 정도를 지역별로 비교하였다.

설 계: 단면 조사 연구

대 상: 각 그룹별로 나이, 성별, 안구장축으로 짝지어진 39안 39명의 한국인

방 법: 사상판 굴곡 지표와 사상판 깊이는 시신경 유두부에서 광학단층촬영을 이용하여 시신경의 상하 지름을 기준으로 균등한 간격을 가지는 7개 부위에서 측정되었다. 상측과 하측 사상판 굴곡 지표 및 사상판 깊이는 상/하 비율을 계산하여 비교하였다.

결 과: 정상군(그룹 1)과 비교하여 사상판 굴곡 지표는 그룹 2에서는 상측과 중간 부위에서, 그룹 3에서는 하측과 중간 부위에서, 그리고 그룹 4에서는 모든 부위에서 더 컸다 ($P \leq 0.004$). 사상판 깊이는 비슷한 결과를 보였으나, 그룹 1과 2 사이에서 상측 부위에서는 차이가 없었다. 사상판 굴곡 지표의 상/하 비율은 그룹 1(1.03)과 2(1.20), 그룹 1과 3(0.79), 그룹 2와 3, 그룹 2와 4(0.96), 그리고 그룹 3과 4에서 차이가 났으나 (all $P < 0.001$), 그룹 1과 4 사이에는 차이가 없었다 ($P = 0.273$). 사상판 깊이의 상/하 비율은 그룹 2와 3 사이에서만 차이가 났다 ($P = 0.002$).

결 론: 개방각녹내장 눈에서 시신경 결손 부위에 따른 사상판 모양의 지역별 차이가 관찰되었다. 사상판 굴곡 지표의 지역별 다양성은 개방각녹내장에서 사상판 모양의 평가를 전반적으로 하는 것보다 지역별로 하는 것이 보다 더 바람직하다는 것을 시사한다.

키워드: 녹내장, 사상판, 반측 결손
학 번: 2017-21254